Energy 226 (2021) 120375

Contents lists available at ScienceDirect

Energy

journal homepage: www.elsevier.com/locate/energy

Lab-scale experimental tests of power to gas-oxycombustion hybridization: System design and preliminary results

Manuel Bailera [a, *], Begoña Peña [a], Pilar Lisbona [b], Julián Marín [a], Luis M. Romeo [a]

[a] Escuela de Ingeniería y Arquitectura. Universidad de Zaragoza, Campus Río Ebro, María de Luna 3, 50018, Zaragoza, Spain
[b] Fundación Agencia Aragonesa para La Investigación y El Desarrollo (ARAID), Zaragoza, Spain

ARTICLE INFO

Article history:
Received 14 October 2020
Received in revised form
24 February 2021
Accepted 12 March 2021
Available online 15 March 2021

Keywords:
Power-to-Gas
Oxycombustion
Methanation
Lab-scale facility

ABSTRACT

Power-to-Gas (PtG) represents one of the most promising energy storage technologies. PtG converts electricity surplus into synthetic natural gas by combining water electrolysis and CO_2 methanation. This technology valorises captured CO_2 to produce a 'carbon neutral' natural gas, while allowing temporal displacement of renewable energy. PtG-Oxycombustion hybridization is proposed to integrate mass and energy flows of the global system. Oxygen, comburent under oxy-fuel combustion, is commonly produced in an air separation unit. This unit can be replaced by an electrolyser which by-produces O_2 reducing the electrical consumption and the energy penalty of the carbon separation process. The aim of this work is to present the design, construction and testing of a methanation reactor at laboratory scale to increase the knowledge of the key component of this system. Experimental data are used to validate the theoretical kinetic model at different operating temperatures implemented in Aspen Plus. CO_2 conversions about 60–80% are found for catalyst temperature between 350 and 550 °C. These values agree well with expected theoretical conversions from the kinetic model.

1. Introduction

Lately, the interest in the promotion of renewables sources to decarbonize the current energy system has strongly increased to mitigate the effects of climate change. As agreed in the United Nations Climate Change Conference in 2015, CO_2 atmospheric concentration must be kept below 450 ppm by the year 2100 in order to limit the global temperature increase below 2 °C (compared to pre-industrial levels) [1]. According to the International Energy Agency, such mitigation target relies on decarbonizing electricity generation and industry [2]. For this reason, the European policy framework for the period 2020–2030 promotes the increase of the share of renewable energy in the electricity sector to 45% by 2030 (so far, a 30.8% share has been reached [3]), while considers carbon capture as the only feasible option to reduce industrial emissions at the required large scale [4]. Furthermore, the "*EU Reference Scenario 2016. Energy, transport and GHG emissions. Trends to 2050*" quantifies the contribution of renewable net electricity generation to 56% by 2050 [5].

However, the massive penetration of renewable energy sources in the energy mix implies large quantities of intermittent energy production in the electricity market. The management of this intermittency (especially in future scenarios) has brought to light the necessity of deploying energy storage systems. Thus, matching energy production and demand becomes a critical challenge for future energy systems. Current energy storage technologies present disadvantages when applied at large scale, such as low energy density and/or limited storage potential. One promising technology to overcome these limitations is the use of Power to Fuels technologies which store excess energy as synthetic fuel that can be used in a future period [6]. The most common synthetic fuel is hydrogen. Electricity is fed to an electrolyser that dissociates water and produces the storable hydrogen. The main barriers to make this process feasible are the high investment costs, the required modifications in infrastructures and the relatively low round-trip efficiency [7].

New alternative fuels produced from hydrogen and carbon dioxide have been proposed to widen the application of hydrogen as energy vector and limit these drawbacks. Methane has stood out in the last years as the main option for Power to Gas (PtG) [8]. This concept uses the stored hydrogen to produce methane via the methanation of CO_2 ($CO_2+4H_2 \leftrightarrow CH_4+2H_2O$, $\Delta H^0_{298} = -165$ kJ/mol).

* Corresponding author.
E-mail addresses: mbailera@unizar.es, manuelbailera@gmail.com (M. Bailera).

https://doi.org/10.1016/j.energy.2021.120375

Nomenclature

Symbols

c_P	specific heat at constant pressure, J/kg·K
d	diameter, m
E_A	activation energy, kJ/mol
k	rate constant, mol/s·g_{cat}
k_0	pre-exponential factor, mol/s·g_{cat}
K_{eq}	equilibrium constant, 1/atm^2
$\boldsymbol{L}$	tube length, m
$\dot{m}$	mass flow, kg/h
n	parameter,
P	pressure, atm
Pr	Prandtl number,
Q	Heat transfer, W
Re	Reynolds number,
r	conversion rate, mol/s·g_{cat}
R	ideal gas constant, kJ/K·mol
T	temperature, K
y	mass fraction

Greek symbols

α	parameter, 1/atm
η_{CH4}	CO_2 conversion to CH_4
λ	thermal conductivity, W/m·K
μ	dynamic viscosity, kg/m·s
ν	kinematic viscosity, m^2/s
ρ	density, m^3/kg

Subscripts and superscripts

act	activation
air	cooling air
bed	bed
eq	equilibrium
ext	external
int	internal
p	particle
reac	reaction
ref	refrigeration
sur	wall surface (reactor; inner annulus)

Power to Gas connects electric and gas networks. This connection allows the storage of renewable electricity surplus and its later utilization to satisfy backup or end-use demand. At the same time, a carbon source is needed for the methanation. Carbon capture technology is required to supply CO_2 for the reaction. This concept may avoid the necessity of carbon storage as CO_2 is valorised for methane production. The resulting methane can be directly consumed by end-users (industry, households, buildings and transport) distributed through the existing gas network, to displace fossil fuels in those applications where the introduction of other renewable energy sources is challenging.

Nevertheless, the high capital cost is still a strong barrier for Power to Gas deployment and the concept is not profitable yet. This unsolved problem was the motivation to propose the concept of Power to Gas-Oxyfuel combustion hybridization (Fig. 1) to better integrate energy and mass flows [9,10]. Some works have investigated the application of this proposal [11] with biomass as fuel [10], in power plants as energy storage [12] or the combination with solid oxide electrolysis [13]. The benefits of this combination have also been theoretically demonstrated [14]. In oxy-fuel combustion, a mixture of pure oxygen and recycled flue gas (mainly CO_2 and H_2O) is the comburent. The electrolyser in the PtG facility which by-produces O_2 may replace the air separation unit (ASU). Thus, the electrical consumption of the ASU may be reduced [9] and no extra energy penalty is associated to the separation of CO_2 from flue gas. Besides, the exothermal heat from methanation can be directly integrated as a useful thermal output of the system or integrated in the thermal power cycle to increase the generation of electricity [12].

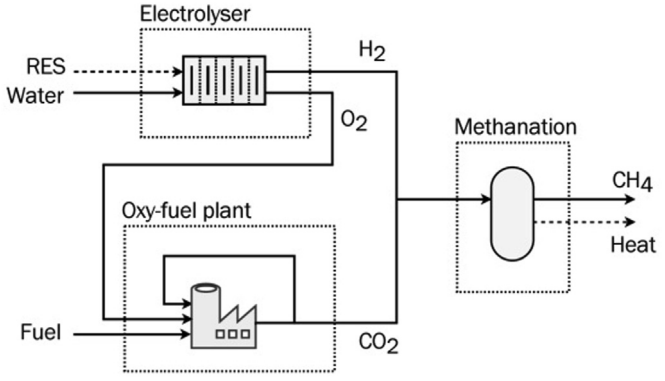

Fig. 1. Conceptual scheme of Power to Gas-Oxyfuel combustion technology.

The core of the process is the methanation reaction. Although some experimental facilities of biological methanation exist [7,8], catalytic methanation in several stage is the preferred via. Catalytic methanation uses active materials like nickel, ruthenium, or cobalt to promote the Sabatier reaction. It is favoured by high pressures and low temperatures, although it can operate between 250 °C and 750 °C, and at pressures between 1 and 100 bar [8]. The main drawbacks are the low tolerance against the presence of impurities in the CO_2 source and the limited flexibility to manage temperature fluctuations caused by load variations [7,8]. Several types of reactors have been proposed in literature to implement the process: adiabatic fixed-bed, cooled fixed-bed, structured reactor, fluidized bed reactor, and three-phase reactor [7,15]. The simplest one is the adiabatic fixed-bed reactor where inlet gases react passing through fixed catalyst layers located inside the reactor. Since high temperature and the presence of steam inhibit the process, from 2 to 5 reactors in series (with intermediate cooling/condensation or recycling loops) are needed to reach CH_4 concentrations above 90% vol. The large amount of energy released inside the reactor also produces hot-spots that can damage the catalyst, and limits the operability under load fluctuations. Others types of reactor with significant performance advantages present a more complex design and first laboratory test rigs are more focused on avoiding problems than increase the conversion efficiency. The experimental reactor is a fixed bed, plug reactor analogous to Refs. [16,17] but the catalyst is dispersed throughout the reactor with quartz wool. In the future, depending on heat transfer limitations, other types of methanation reactor could be tested as heat pipes [18] or micro-channel reactors [19].

A Ru-based catalyst 0.5% wt in 3 mm particles supported with alumina has been used. This catalyst is similar to those used in Ref. [20] with different diameters (100, 800 and 2300 μm vs pellets) Other types of catalyst have been also considered in literature with good results, up to 75% CO_2 conversion using an isothermal plug-

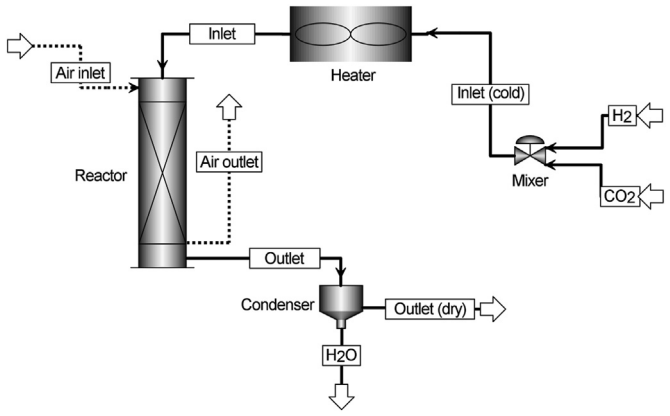

Fig. 2. Model of the methanation plant in Aspen Plus (air mass flowrate is calculated in EES).

flow reactor with Ni [21,22]. Also others Ni-compounds (based on Mn, Ce, Zr, Mg, K, Zn, V) have been studied. Results show that the combination of Ni−V/Al catalyst with Al_2O_3 as support performs the highest CO methanation activity due to the largest Ni sites [23]. Different studies have proven the optimum ratio Mn/Ni between some of the metal elements, as [24] for Mn/Ni about 0.25, and also in other combinations with Ni + Ce [25]. Most of these catalysts, and also Ni_3Fe [26] or Ni/Al [27], were supported in Al_2O_3 but lately some researchers have started to look for alternative supports as zeolites synthesized from waste fly ashes from the energy sector [28].

The aim of this work is to characterize experimental SNG production under different temperatures with a single reactor with no gas recirculation, operating at 1 bar and 300-400 °C, in plug flow with non-diluted mixtures H_2/CH_4, using as Ru-based catalyst dispersed throughout the reactor with quartz wool. The objective is to obtain data to validate the simulation work developed to study the integration of PtG-Oxycombustion in different applications. As reactor temperatures are assumed to vary along the axis affecting the conversion rate, the next stage would be to perform an optimization similar to Ref. [29] where axial temperatures would be controlled to avoid kinetic and/or thermodynamic limitations, and maximize the conversion rate in the reactor.

2. Methodology

Both, simulation and experimental tasks have been developed in this study. The modelling of the methanation plant in Aspen Plus was used to size the lab-scale plant during the design of the facility. A heat transfer model was also developed to estimate the cooling air mass flow and the temperature at different points of the reactor. The kinetic model of the methanation process was also implemented to be validated through experimental results obtained in the lab-scale plant. This section details both models and describes the resultant experimental lab facility.

2.1. Methanation plant modelling

Aspen Plus software has been used to model the methanation plant assuming isothermal and steady state operation in the reactor (Fig. 2). The developed simulations use the RKSMHV2 property method provided by Aspen Plus. This package is based on the Redlich-Kwong-Soave equation-of-state and modified Huron-Vidal mixing rules, which are valid for the tested temperatures and pressures. Moreover, the EES (Engineering Equation Solver) has been used to perform the calculations on heat transfer to size the mass flow of air required in the cooling system.

2.1.1. Reaction kinetics

The kinetic model chosen for the simulation was published by Falbo et al. [30]. This model was developed for the same commercial catalyst used in our plant (0.5 wt% Ru/Al_2O_3, Aldrich 206,199 CAS = 1344−28−1, MDL = MFCD00011207). They modified the model proposed by Lunde et al. [31] by explicitly accounting for the dependence of the partial pressure of water [30].

The conversion rate of CO_2 is given by Eq. (1),

$$r_{CO2} = \frac{k}{1+\alpha\cdot[P_{H2O}]}\cdot\left([P_{CO2}]^n[P_{H2}]^{4n} - \frac{[P_{CH4}]^n[P_{H2O}]^{2n}}{(K_{eq}(T))^n}\right), \quad (1)$$

where $[P_i]$ is the partial pressure of component i, the parameter $\alpha = 0.91\ \text{atm}^{-1}$ gives the dependence on the water partial pressure, the coefficient n is adjusted to 0.152 according to experiments, and the dependence of the equilibrium constant with temperature is correlated by Eq. (2).

$$K_{eq}(T) = \exp\left[\frac{1}{1.987}\cdot\left(\frac{56000}{T^2}+\frac{34633}{T}-16.4\cdot\ln T+0.00557\cdot T\right)+33.165\right]. \quad (2)$$

The rate constant, k, follows the Arrhenius equation, Eq. (3),

$$k = k_0\cdot\exp\left(-\frac{E_A}{R\cdot T}\right), \quad (3)$$

where the pre-exponential factor k_0 is 95.43 mol/s·g_{cat}, and the activation energy E_A is 75.3 kJ/mol.

In order to implement this kinetic model in Aspen Plus, the generalized Langmuir-Hinshelwood-Hougen-Watson (LHHW) model type is selected. The reacting phase is set in 'Vapor' under a weight rate basis ('Cat (wt)'). The kinetic expression must be placed as Eq. (4),

$$r = \frac{[\text{Kinetic factor}]\cdot[\text{Driving force}]}{[\text{Adsorption}]}, \quad (4)$$

where the [Kinetic factor], the [Driving force expression] and the [Adsorption expression] follows Eq. (5), Eq. (6) and Eq. (7), respectively. In these equations, the corresponding terms of Eq. (1) are included for clarification purposes.

$$[\text{Kinetic factor}] \equiv k\cdot T^n\cdot\exp\left(-\frac{E}{R\cdot T}\right) = k_0\cdot\exp\left(-\frac{E_A}{R\cdot T}\right), \quad (5)$$

$$[\text{Driving force}] \equiv k_1\prod_{i=1}^{N}C_i^{\alpha_i} - k_2\prod_{j=1}^{N}C_j^{\beta_j} = [P_{CO2}]^n[P_{H2}]^{4n} - \frac{[P_{CH4}]^n[P_{H2O}]^{2n}}{(K_{eq}(T))^n}, \quad (6)$$

$$[\text{Adsorption}] \equiv \left[\sum_{i=1}^{M}k_i\left(\prod_{j=1}^{N}C_j^{\nu_j}\right)\right]^m = 1+\alpha\cdot[P_{H2O}], \quad (7)$$

The concentration C_i is expressed in a partial pressure basis in Aspen Plus, so its units in Eq. (6) and Eq. (7) are [N/m^2]. Conversion of units must be performed in the driving force's terms to adapt the

model of Falbo et al. (e.g., k_1 is not 1 in Eq. (6), despite what might be inferred from direct comparison with the corresponding term of Eq. (1)). Besides, the temperature-dependent expression of k_i that appear in Eq. (6) and Eq. (7) must be placed in the form of Eq. (8).

$$k_i = \exp(A_i)\cdot\exp\left(\frac{B_i}{T}\right)\cdot T^{C_i}\cdot\exp(D_i\cdot T) \quad \text{for } i = 1,\ 2, \tag{8}$$

The parameters adapted to the Aspen Plus equations are gathered in Table 1.

The results from Aspen Plus are compared with experimental results of Falbo et al. [30] in Fig. 3, in order to check that the kinetic model was properly implemented. In the experiments of Falbo et al. a tubular fixed-bed reactor was used, with 23 cm in length and 1.1 cm in diameter. The amount of catalyst used was 0.375 g, diluted with α-Al_2O_3 at 1 to 1 volumetric dilution. The Aspen Plus model has been validated for the range 250–410 °C, 1–7 bar and GHSV between 3.75 and 10.00 l (STP)/h/g_{cat}.

2.1.2. Cooling sizing model

Sizing of air cooling system has been carried out through a 1D thermal model, considering radial symmetry and constant variables in axial direction. Therefore, surface temperature, as well as heat transfer coefficients, are considered to be constant along the heat exchange surface. The cooling air is supplied from a compressed air line, assumed to be at 3.5 bar and 23 °C, while the reactor is considered isothermal under steady state operation.

Properties of gas mixture at inlet and outlet of the reactor are calculated from the molar fractions of CO_2, CO, H_2O and CH_4. It should be noted that these molar fractions at the outlet of the reactor corresponds to the maximum theoretical conversion achieved at the pressure and temperature considered.

The specific heat and density of each gas mixture are calculated from the mass fractions (y_i) as $\overline{c_P} = \sum_i y_i \cdot c_{P,i}$ and $\overline{\rho} = \sum_i y_i \cdot \rho_i$. For the calculation of the dynamic viscosity, the Wilke mixing rule can be applied at low pressures (Eq. (9) and Eq. (11)), while for thermal conductivity the equivalent rule of Wassiljeva, Mason, and Saxena is applicable (Eq. (10) and Eq. (11)) [32].

$$\overline{\mu} = \sum_i \frac{y_i \cdot \mu_i}{\sum_k y_k \cdot F_{ik}} \tag{9}$$

$$\overline{\lambda} = \sum_i \frac{y_i \cdot \lambda_i}{\sum_k y_k \cdot F_{ik}} \tag{10}$$

$$F_{ik} = \frac{\left[1 + \sqrt{\mu_i/\mu_k}\cdot\sqrt[4]{M_k/M_i}\right]^2}{\sqrt{8\cdot\left(1 + M_i/M_k\right)}}, \quad M_i:\ \text{molar mass} \tag{11}$$

The Prandtl number and kinematic viscosity are calculated from the involved mean properties of the inlet-outlet gas mixtures previously obtained, as $\overline{\nu} = \overline{\mu}/\overline{\rho}$ and $\overline{Pr} = \overline{c_P}\cdot\overline{\mu}/\overline{\lambda}$.

The heat transfer model includes the calculation of three convection heat transfer coefficients: cooling air – surface of the reactor, surface of the reactor – gas mixture and gas mixture – catalyst particles. The thermal resistance associated to the stainless steel wall of the reactor is negligible. For the calculation of the convection coefficient of the cooling air flow in the annular duct, the outer wall of the annulus is assumed adiabatic and the inner wall is considered isothermal [33]. The air properties are calculated at bulk temperature of the fluid. Regarding the inner convection coefficient, the Hausen correlation is applied as laminar flow, given the small occupancy ratio inside the reactor. The fluid properties are calculated at bulk temperature as mean value of that obtained for the gas mixture at inlet and outlet of the reactor. The entry region effects are considered in both cases. The properties evaluated at the film temperature were used in the correlation for external flow past a sphere is used, as well as in the correlation for the heat transfer between particles and gas mixture. According to that, the cooling air mass flow and the mean temperatures of air ($T_{o,air}$), reactor wall surface (T_{sur}) and catalyst particles (T_p) are estimated.

Table 1
Implementation of the kinetic model in Aspen Plus (Rate basis: weight. Concentration basis: partial pressure).

Aspen Plus	Parameter	*Value*				*Units*
[Kinetic factor]						
Pre-exponential factor	K	95.43				$kgmole/kg_{cat}\cdot s$
Temperature exponent	N	0				–
Activation energy	E	75.3				kJ/mol
[Driving force] Term 1			**[Driving force] Term 2**			
Exponent (CO_2)	α_{CO2}	0.152	Exponent (CO_2)	β_{CO2}	0	–
Exponent (H_2)	α_{H2}	0.608	Exponent (H_2)	β_{H2}	0	–
Exponent (CH_4)	α_{CH4}	0	Exponent (CH_4)	β_{CH4}	0.152	–
Exponent (H_2O)	α_{H2O}	0	Exponent (H_2O)	β_{H2O}	0.304	–
Coefficient in k_1	A_1	−8.75983	Coefficient in k_2	A_2	−10.296976	–
Coefficient in k_1	B_1	0	Coefficient in k_2	B_2	−2649.3286	K
Coefficient in k_1	C_1	0	Coefficient in k_2	C_2	1.2545	–
Coefficient in k_1	D_1	0	Coefficient in k_2	D_2	$-4.26089\cdot10^{-4}$	1/K
[Adsorption]						
Adsorption exponent	M	1	–			
[Adsorption] Term 1			**[Adsorption] Term 2**			
Exponent (CO_2)	ν_{CO2}	0	Exponent (CO_2)	ν_{CO2}	0	–
Exponent (H_2)	ν_{H2}	0	Exponent (H_2)	ν_{H2}	0	–
Exponent (CH_4)	ν_{CH4}	0	Exponent (CH_4)	ν_{CH4}	0	–
Exponent (H_2O)	ν_{H2O}	0	Exponent (H_2O)	ν_{H2O}	1	–
Coefficient in k_1	A_1	0	Coefficient in k_2	A_2	−11.4317	–
Coefficient in k_1	B_1	0	Coefficient in k_2	B_2	0	K
Coefficient in k_1	C_1	0	Coefficient in k_2	C_2	0	–
Coefficient in k_1	D_1	0	Coefficient in k_2	D_2	0	1/K

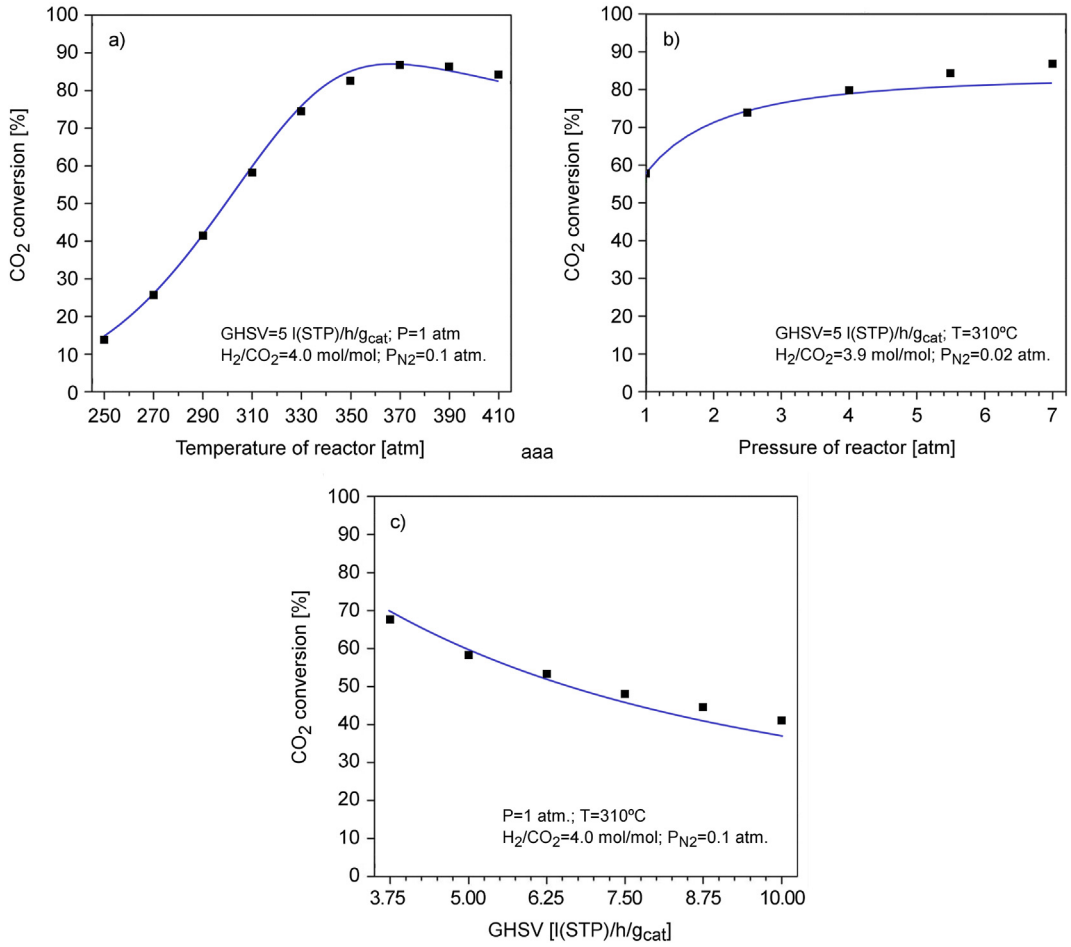

Fig. 3. Comparison between the Aspen Plus model (line) and Falbo et al. experiments [30] *(dots).*

2.2. Methanation test facility

The laboratory scale facility consists of three complementary systems: generator of hydrogen and oxygen, methanation reactor, and oxy-combustion chamber. The generator of hydrogen and oxygen is a PEM electrolyser (model GREENMH2 Hart 400 W 66 lN/h) powered by photovoltaic panels. The hydrogen produced is stored in a tank to be further mixed with CO_2 to produce methane in the methanation reactor. Moreover, an oxy-fuel burner is available to consume this renewable methane and perform tests on combustion processes. In this work, we only focus on the methanation test facility (description, model and results).

The laboratory methanation facility (Fig. 4) consists of a gas premixer (in these experimental tests we use bottled gases), a ceramic heater to pre-heat the reagent mixture up to 300–400 °C, a fixed bed reactor (with electrical heating and air cooling), a water condenser and a burner to co-fire the synthetic methane with butane. For cleaning and heating purposes, the facility also includes a N_2 entry. Pressure, temperature and mass flows are measured with standard instrumentation at different points of the installation, while the gas composition is measured with a gas analyzer before and after the methanation stage. The gas analyzer comprises a "CALOMAT 6" model from Siemens for the measurement of the H_2 content (measured by thermal conductivity), and a "ULTRAMAT 23" model from Siemens for the measurement of CO_2 and CH_4 (infrared detector). The operation parameters, in particular mass flows of reactants, are controlled by an advanced Labview system, which also records the on-line measurements.

The use of bottled gases avoids undesired impurities inside the reactor. Besides, the mass flow controllers for the H_2 and CO_2 allow the regulation of the mass fractions to the stoichiometric ratio. The gas is stored at 6 bar inside the bottles, but the pressure is set in the operating value through a pressure reducer. Hydrogen flow ranges from 335 to 1796 l/h, equivalent to 1–5 kW_{H2} input, while CO_2 flow varies from 84 to 446 l/h.

The reactor is a "double pipe" design with parallel flows (air as cooling fluid in the outer side) and equipped with two CaF_2 crystal viewports. The catalyst fixed bed is located inside the tube of $L = 590$ mm length, $d_{int} = 33.4$ mm inner diameter and 4.45 mm thickness. The cooling air flows through the annular space, being 100 mm the outer diameter of the shell. The inner tube is filled with 50 g of commercial pellets of alumina impregnated with Ruthenium (0.5 wt% Ru/Al_2O_3, cylindrical pellets of 3.2 mm in length and 3 mm in diameter, with a weight of 0.05 g/pellet) and quartz wool. A total of 9 thermocouples are distributed along the reactor length (5 cm of separation), in contact with the wall of the inner tube (wall of the tube containing the fixed bed) (see Fig. 5). After methanation stage, the resultant flow is driven to a condenser to reduce the water content as much as possible before the gas analyzer intake. Finally, the produced gas is burnt in a butane pilot flame.

The lab-scale experimental plant was operated to find stationary operation points which lead to stationary carbon conversions in the reactor and constant temperatures at the thermocouples located at different points of the facility. Carbon conversion was easily

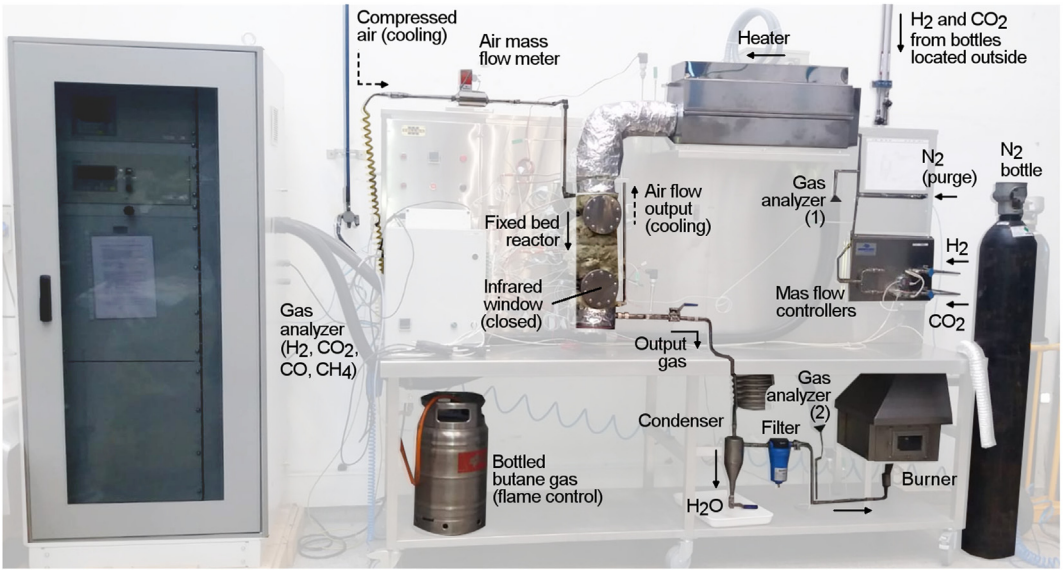

Fig. 4. Methanation test facility.

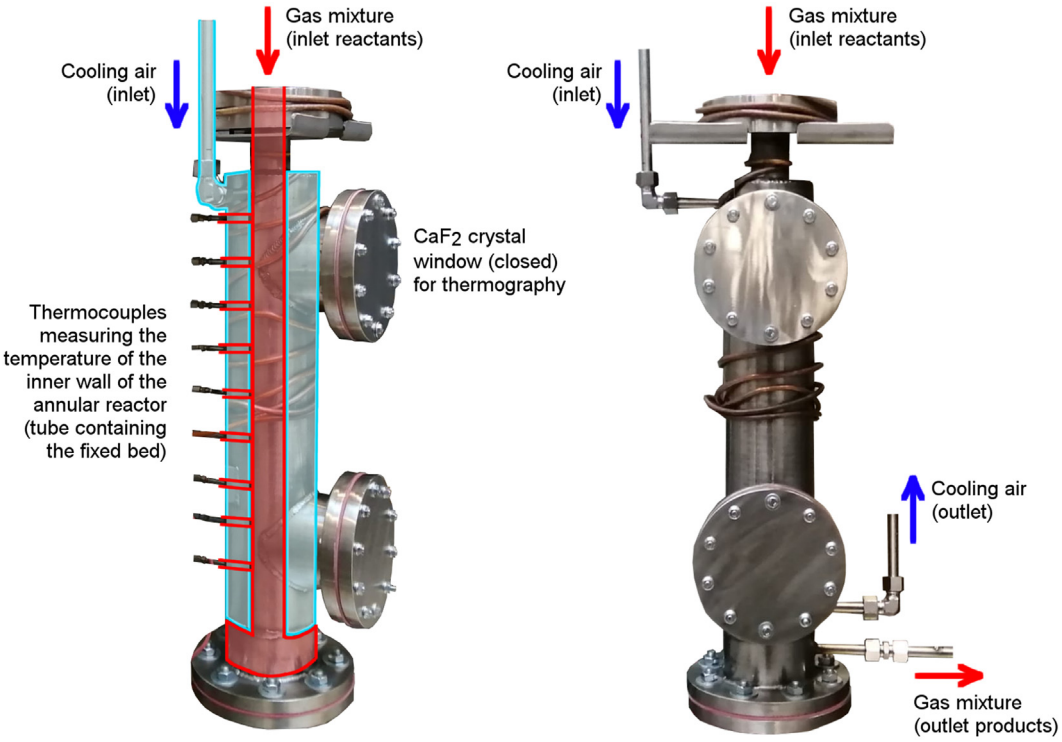

Fig. 5. Methanation reactor (without external insulation).

calculated with the information provided by the gas analyzer sampling before and after methanation stage while reactor temperature was registered on-line by the K-type microthermocouples attached to the reactor outer surface.

3. Results

The fixed bed reactor in the methanation test facility is 400 mm in length and 33.4 mm in diameter. The mole flow of H_2 is set at 54 kmol/s (i.e., 1 kW_{LHV}) and the flow of CO_2 at 13.7 kmol/s (stoichiometric proportion). This section includes the theoretical results obtained from the model previously presented and the experimental results from the lab-scale facility loaded with 50 g of catalyst.

3.1. Simulation results

A sensitivity analysis has been performed under isothermal operating temperature inside the reactor, at three different loads of catalyst (50 g, 100 g and 150 g) and constant stoichiometric H_2/CO_2

ratio. The carbon conversion and excess heat in the reactor are calculated and represented for different operating temperatures.

The maximum CO_2 conversions are reached at 390 °C, 360 °C, and 340 °C isothermal operating temperatures, for catalyst loads inside the reactor of 50 g, 100 g and 150 g, respectively (Fig. 6). These maximum conversions achieve values of 83.6%, 87.5% and 88.9% for the three different situations of catalyst loading.

The heat to be removed from the reactor under these operating points to maintain isothermal conditions is 0.160 kW, 0.166 kW and 0.168 kW, respectively. The cooling air mass flow and the mean temperatures of air ($T_{o,air}$), wall surface (T_{sur}) and catalyst particles (T_p) calculated from the thermal model (see section 3.1.2) are presented in Table 2. The heat released in the reaction is assumed to be fully transferred to the cooling air to keep isothermal conditions in the reactor. It should be noted that there is a difference of almost 100 °C between the temperature of surface of the inner tube of the annulus (i.e., where the thermocouples are installed) and the temperature of the particle (on which the reaction takes place).

The results of the simulation for the whole plant are presented in Fig. 7, for the three optimized cases. The methane concentration in the dried gas varies between 52% and 64%, as there is only one methanation stage in the test facility. The methane content could be increased to 95% by adding subsequent reactors (required CH_4 content in the Spanish legislation for grid injection of the gas [34]).

3.2. Methanation experimental results

The mass flowrate of hydrogen and carbon dioxide in these experimental tests were 0.03 and 0.16 kg/h, respectively, preserving a constant stoichiometric H_2/CO_2 ratio of methanation reaction. The temperature of the gas mixture entering into the reactor ranged between 225 and 245 °C. The reactor was heated by electric resistances to achieve the desired operating temperature in the fixed bed. Then, the electric resistances were turn off and the cooling system was used to reach stationary states. A total of ten stationary operation points for 50 g catalyst load were studied. The temperature of the reactor wall varied from 244 to 442 °C (measured with the thermocouples), corresponding to catalyst temperatures of 344–442 °C according to the heat transfer model (see Table 3). The time (t_{act}) and temperature of activation ($T_{act,\ reac}$) of the catalyst are gathered in the first two columns of Table 3. The temperature measured in the wall surface is denoted as T_{sur}, and it can be considered uniform in the reaction zone given its low standard deviation ($\sigma(T_{sur})$). The time duration of the steady state operation (t_{test}), outlet volume fractions, mass flow of cooling air ($\dot{m}_{air}$), net refrigeration (Q_{ref}) and CO_2 conversion to methane (η_{CH4}) are also shown.

In the simulation results presented in section 3.1, the maximum conversion of CO_2 to methane (50 g catalyst) was 83.6%, at 390 °C catalyst temperature, with a cooling requirement of 160 W corresponding to 5 kg/h of air. In our experiments, the highest conversion was achieved at test #3, #5 and #6, obtaining 79.0–79.4% conversion, at 267–312 °C wall temperature (i.e., about 367–412 °C catalyst temperature), and requiring 1.2–6.4 kg/h of air to evacuate 30–202 W. Deviations due to the real non-isothermal and non-adiabatic conditions of the reactor were expected, and yet the experimental results seems to fit well the simulation results as a first approach.

Regarding the whole set of experiments of Table 3 (10 steady states for catalyst temperature between 344 and 442 °C), the corresponding CO_2 conversion to methane is presented in Fig. 8. Fig. 8 illustrates the CO_2 conversion versus catalyst temperature (bottom abscissa axis) and reactor wall temperature (upper abscissa axis), comparing the equilibrium, the results of the kinetic model, and the experimental tests.

The equilibrium for the CO_2 conversion to any product (i.e., to CH_4 or CO) is depicted with a red dashed line, while the equilibrium for the CO_2 conversion to methane is depicted with a blue dashed line. It can be seen that the appearance of CO in the system seems to me remarkable from about 500 °C catalyst temperature. The simulated behavior provided by the kinetic model is depicted with a solid black line. According to Falbo et al. [30], the kinetic model is valid up to 410 °C as minimum. Still, it seems to fit properly well up to about 470 °C. From 470 °C ahead, the kinetic model overestimated the CH_4 production since the reaction rate does not consider the CO formation (see Eq. (1)). Our experimental results are depicted as square dots in Fig. 8, corresponding each point to one experimental steady state from Table 3 (the reactor is considered isothermal at each test due to the low standard deviation in the wall temperature measured). The experimental points and the predictions from the simulation fit quite well with a difference near to 100 °C between both axes. This figure is quite near to the temperature difference estimated by the heat transfer model between particle and reactor wall under isothermal conditions. It should be noted that experimental results fit properly the kinetic model up to 470 °C, and then logically follows the blue dashed line corresponding to the equilibrium of CH_4 formation (instead of the overestimation of the kinetic model).

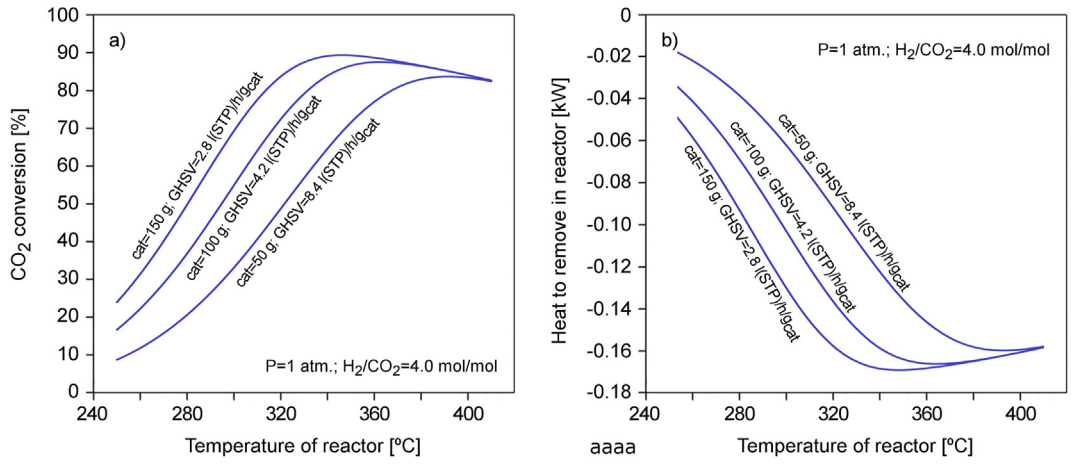

Fig. 6. Simulation results of the methanation test facility at different loads of catalyst: a) CO_2 conversion and b) Heat to be removed from reactor vs. isothermal operating temperature.

Table 2
Operating conditions for simulation analysis (outlet gas composition in dry basis).

m_{cat} (g)	T_{reac} (°C)	T_p (°C)	T_{sur} (°C)	CO_2 (%)	H_2 (%)	CH_4 (%)	$\dot{m}_{air}$ (kg/h)	$T_{o,air}$ (°C)	Q (W)	η_{CH4} (%)
50	390	413	325	10.2	37.7	52.1	5	136.8	160	83.6
100	360	372	288	8.6	31.2	60.2	9	88.6	166	87.5
150	340	349	265	8.0	27.8	64.2	14	65.7	168	88.9

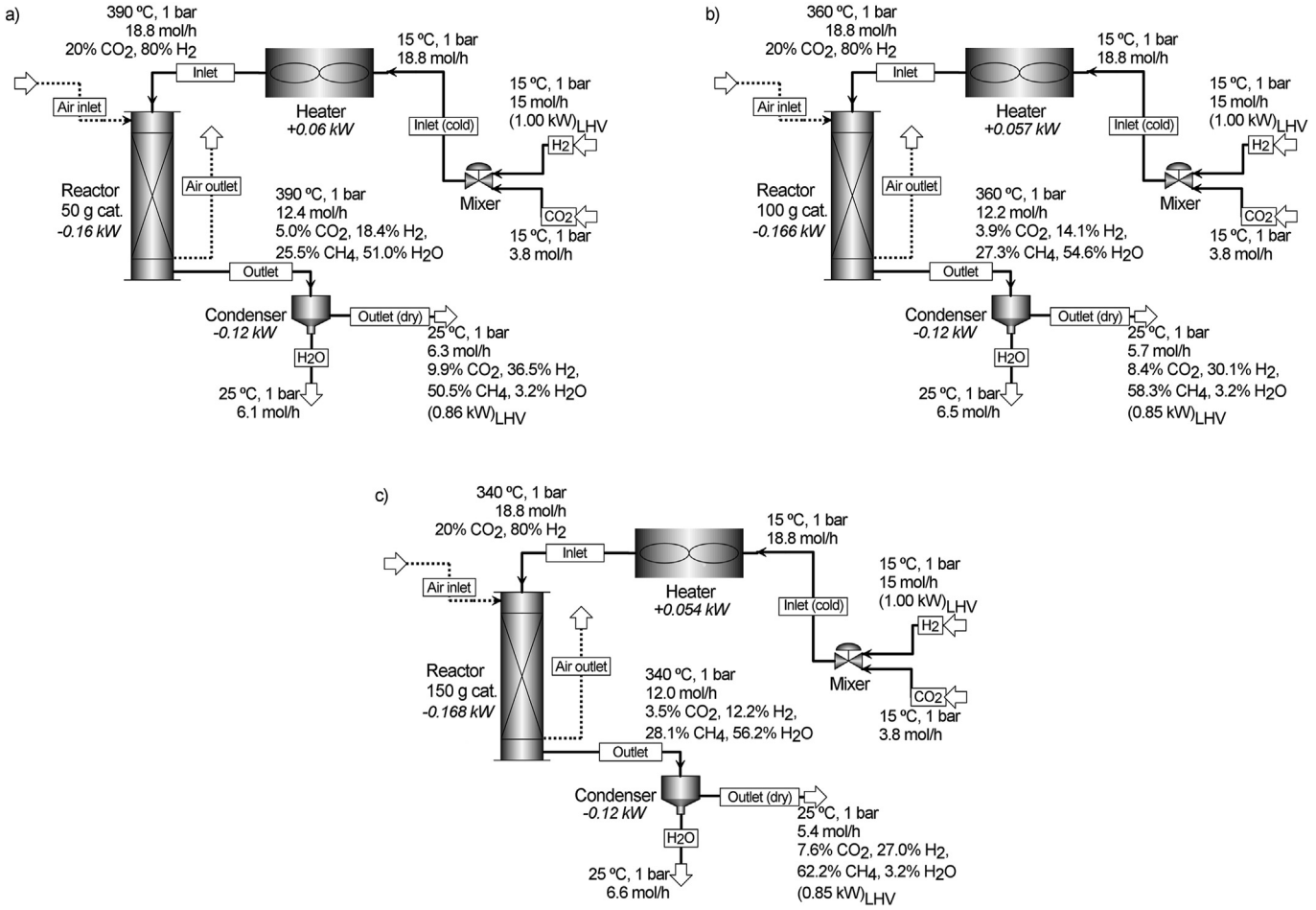

Fig. 7. Simulation of the methanation plant at a) 50 g, b) 100 g, and c) 150 g catalyst load.

Table 3
Operating conditions of preliminary tests with 50 g catalyst load (outlet gas composition in dry basis).

Test	t_{act} (min)	$T_{act,\ reac}$ (°C)	T_{sur} (°C)	$\sigma(T_{sur})$ (%)	t_{test} (min)	CO_2 (%)	H_2 (%)	CH_4 (%)	$\dot{m}_{air}$(kg/h)	Q_{ref} (W)	η_{CH4} (%)
1	61	309	244	1.7	15	11.6	53.9	31.7	3.0	53	73.2
2	34	368	259	4.8	5	16.5	44.2	37.5	14.1	544	69.5
3	61	309	267	7.1	15	10.3	48.1	39.4	6.4	192	79.3
4	37	324	288	3.7	30	11.5	47.7	38.5	3.5	107	77.0
5	61	309	308	1.5	20	10.2	48.0	39.4	1.2	30	79.4
6	61	309	312	4.9	20	10.3	48.4	38.7	5.0	202	79.0
7	37	324	339	1.0	5	11.4	46.7	39.1	3.0	84	77.3
8	37	314	378	1.1	30	11.3	53.5	32.0	0.0	0	73.9
9	34	368	426	3.0	4	21.2	52.0	24.3	3.2	90	53.4
10	34	368	442	1.7	3	19.5	49.2	27.4	0.0	0	58.4

The improvement of the model to emulate non-isothermal conditions in the gas mixture is under development and will be validated with the experimental data in future works. Additionally, a multipoint temperature sensor will be installed in the lab-scale facility to obtain information of the real temperature at the reaction site inside the reactor.

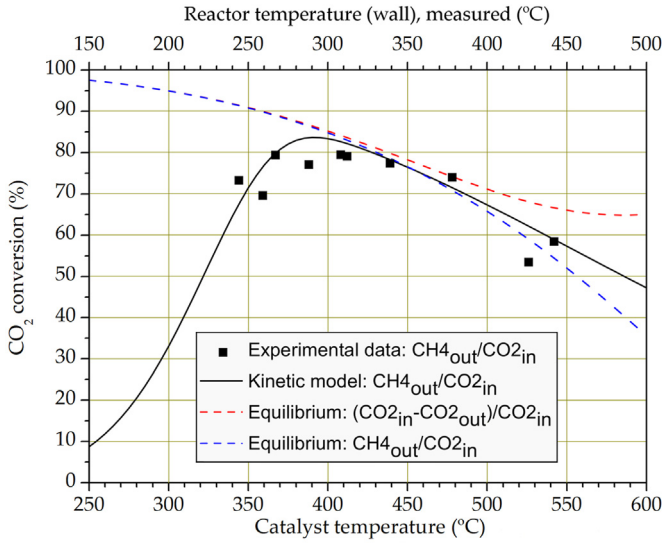

Fig. 8. Experimental results (10 isothermal steady states) and simulation of the methanation reactor at 50 g catalyst load, versus the isothermal temperature of operation.

4. Conclusions

The concept of PtG-Oxycombustion hybridization would facilitate the deployment of PtG technologies as it makes use of the oxygen by-produced in the electrolyzer to avoid energy penalty in the CO_2 separation process. A methanation reactor at laboratory scale has been developed to validate the theoretical models used to study the integration of PtG-Oxycombustion in different applications with the aim of developing this technological option.

This work has presented the detailed design of the lab-scale system based on a single reactor with no gas recirculation, operating at 1 bar and 300-400 °C. The reactor operates in plug flow with non-diluted mixtures of H_2/CO_2, using Ru-based catalyst dispersed throughout the reactor with quartz wool. An air cooling system is available to remove the large amount of heat produced during the reaction.

Simulation results show that CO_2 conversion depends on the operating temperature in the range 300–400 °C. The maximum theoretical CO_2 conversion, 83.6%, is reached at 390 °C isothermal operating temperatures for catalyst loads of 50 g. The heat to be removed from the reactor under that condition is 0.160 kW. Since no measure of the catalyst temperature is available, a heat transfer analysis has been proposed to estimate this temperature, based on the experimental measures of the temperature at the outlet wall of reactor (differences between both temperatures in the range of 100 °C were obtained). Experimental CO_2 conversions in the range 60–80% were found for catalyst temperature between 350 and 550 °C (i.e., reactor wall temperature between 250 and 450 °C). These values agreed well with expected theoretical conversions from the kinetic model.

These experimental results are quite promising since the highest possible conversions for a given load of catalysts have been achieved in the facility. It points out the suitability of the reactor design for this scale of methane production and will allow the performance of further experimental tests under modified operating conditions (e.g., temperature, pressure, gas composition, presence of impurities).

Credit author statement

Manuel Bailera: Conceptualization, Methodology, Software, Validation, Formal analysis, Investigation, Writing – original draft, Writing – review & editing, Visualization. Begoña Peña: Conceptualization, Methodology, Software, Validation, Formal analysis, Investigation, Writing – original draft, Writing – review & editing. Pilar Lisbona: Conceptualization, Investigation, Writing – original draft, Writing – review & editing. Julián Marín: Methodology, Formal analysis, Investigation. Luis M Romeo: Conceptualization, Investigation, Writing – original draft, Writing – review & editing, Supervision, Project administration, Funding acquisition.

Declaration of competing interest

The authors declare that they have no known competing financial interests or personal relationships that could have appeared to influence the work reported in this paper.

Acknowledgments

The work described in this paper is supported by the R + D Spanish National Program from Ministerio de Economía y Competitividad, MINECO (Spanish Ministry of Economy and Competitiveness) and the European Regional Development Funds (European Commission), under project ENE2016-76850-R.

This work has also been supported by the Government of Aragon (Research Group DGA T46_17 R) and co-financed by FEDER 2014–2020 “Construyendo Europa desde Aragón" (ALEN OXY-PtG).

References

[1] Anderson TR, Hawkins E, Jones PD. CO2, the greenhouse effect and global warming: from the pioneering work of Arrhenius and Callendar to today's Earth system models. Endeavour 2016;40:178–87. https://doi.org/10.1016/j.endeavour.2016.07.002.

[2] International Energy Agency. CO2 emissions from fuel combustion. 2015. https://doi.org/10.1787/co2_fuel-2015-en.

[3] Report from the commission to the European parliament, the council, the European economic and social committee and the committee of the regions - renewable energy progress report. European Commission; 2015.

[4] European Commission. A policy framework for climate and energy in the period from 2020 to 2030. 2014.

[5] Capros P, Vita A De, Tasios N, Siskos P, Kannavou M, Petropoulos A, et al. EU reference scenario 2016: energy, transport and GHG emissions. Trends to 2050. European Union; 2016. https://doi.org/10.2833/9127.

[6] Vandewalle J, Bruninx K, D'haeseleer W. Effects of large-scale power to gas conversion on the power, gas and carbon sectors and their interactions. Energy Convers Manag 2015;94:28–39. https://doi.org/10.1016/j.enconman.2015.01.038.

[7] Götz M, Lefebvre J, Mörs F, McDaniel Koch A, Graf F, Bajohr S, et al. Renewable Power-to-Gas: a technological and economic review. Renew Energy 2016;85:1371–90.

[8] Bailera M, Lisbona P, Romeo LM, Espatolero S. Power to Gas projects review: lab, pilot and demo plants for storing renewable energy and CO2. Renew Sustain Energy Rev 2017;69:292–312. https://doi.org/10.1016/j.rser.2016.11.130.

[9] Bailera M, Lisbona P, Romeo LM. Power to gas-oxyfuel boiler hybrid systems. Int J Hydrogen Energy 2015. https://doi.org/10.1016/j.ijhydene.2015.06.074.

[10] Bailera M, Lisbona P, Romeo LM, Espatolero S. Power to Gas-biomass oxycombustion hybrid system: energy integration and potential applications. Appl Energy 2016;167:221–9. https://doi.org/10.1016/j.apenergy.2015.10.014.

[11] Israel J, Rachow F, Müller K, Beukert G, Schmeiber D. Upscaling of catalytic CO2 methanation to a demonstration plant. Int. GeoEn Conf. 2012;2012.

[12] Bailera M, Kezibri N, Romeo LM, Espatolero S, Lisbona P, Bouallou C. Future applications of hydrogen production and CO2 utilization for energy storage: hybrid Power to Gas-Oxycombustion power plants. Int J Hydrogen Energy 2017:1–8. https://doi.org/10.1016/j.ijhydene.2017.02.123.

[13] Eveloy V. Hybridization of solid oxide electrolysis-based power-to-methane with oxyfuel combustion and carbon dioxide utilization for energy storage. Renew Sustain Energy Rev 2019;108:550–71. https://doi.org/10.1016/j.rser.2019.02.027.

[14] Romeo LM, Bailera M. Design configurations to achieve an effective CO2 use and mitigation through power to gas. J CO2 Util 2020;39:101174. https://

doi.org/10.1016/j.jcou.2020.101174.
[15] Rönsch S, Schneider J, Matthischke S, Schlüter M, Götz M, Lefebvre J, et al. Review on methanation - from fundamentals to current projects. Fuel 2016;166:276–96.
[16] Gruber M, Weinbrecht P, Biffar L, Harth S, Trimis D, Brabandt J, et al. Power-to-Gas through thermal integration of high-temperature steam electrolysis and carbon dioxide methanation - experimental results. Fuel Process Technol 2018;181:61–74. https://doi.org/10.1016/j.fuproc.2018.09.003.
[17] Lefebvre J, Bajohr S, Kolb T. A comparison of two-phase and three-phase CO2 methanation reaction kinetics. Fuel 2019;239:896–904. https://doi.org/10.1016/j.fuel.2018.11.051.
[18] Neubert M, Hauser A, Pourhossein B, Dillig M, Karl J. Experimental evaluation of a heat pipe cooled structured reactor as part of a two-stage catalytic methanation process in power-to-gas applications. Appl Energy 2018;229:289–98. https://doi.org/10.1016/j.apenergy.2018.08.002.
[19] Chwoła T, Spietz T, Więcław-Solny L, Tatarczuk A, Krótki A, Dobras S, et al. Pilot plant initial results for the methanation process using CO2 from amine scrubbing at the Łaziska power plant in Poland. Fuel 2020;263:116804. https://doi.org/10.1016/j.fuel.2019.116804.
[20] Porta A, Falbo L, Visconti CG, Lietti L, Bassano C, Deiana P. Synthesis of Ru-based catalysts for CO 2 methanation and experimental assessment of intra-porous transport limitations. Catal Today 2019. https://doi.org/10.1016/j.cattod.2019.01.042.
[21] Marocco P, Morosanu EA, Giglio E, Ferrero D, Mebrahtu C, Lanzini A, et al. CO2 methanation over Ni/Al hydrotalcite-derived catalyst: experimental characterization and kinetic study. Fuel 2018;225:230–42. https://doi.org/10.1016/j.fuel.2018.03.137.
[22] Champon I, Bengaouer A, Chaise A, Thomas S, Roger AC. Carbon dioxide methanation kinetic model on a commercial Ni/Al2O3 catalyst. J CO2 Util 2019;34:256–65. https://doi.org/10.1016/j.jcou.2019.05.030.
[23] Le TA, Kim J, Kang JK, Park ED. CO and CO2 methanation over M (M[dbnd]Mn, Ce, Zr, Mg, K, Zn, or V)-promoted Ni/Al@Al2O3 catalysts. Catal Today 2019. https://doi.org/10.1016/j.cattod.2019.08.058.
[24] Vrijburg WL, Garbarino G, Chen W, Parastaev A, Longo A, Pidko EA, et al. Ni-Mn catalysts on silica-modified alumina for CO2 methanation. J Catal 2020;382:358–71. https://doi.org/10.1016/j.jcat.2019.12.026.
[25] Qin Z, Zhao Y, Yi Q, Shi L, Li C, Yan X, et al. Methanation of coke oven gas over Ni-Ce/γ-Al2O3 catalyst using a tubular heat exchange reactor: pilot-scale test and process optimization. Energy Convers Manag 2020;204:112302. https://doi.org/10.1016/j.enconman.2019.112302.
[26] Farsi S, Olbrich W, Pfeifer P, Dittmeyer R. A consecutive methanation scheme for conversion of CO2 – a study on Ni3Fe catalyst in a short-contact time micro packed bed reactor. Chem Eng J 2020;388:124233. https://doi.org/10.1016/j.cej.2020.124233.
[27] Le TA, Kim J, Kang JK, Park ED. CO and CO2 methanation over Ni/Al@Al2O3 core–shell catalyst. Catal Today 2019. https://doi.org/10.1016/j.cattod.2019.09.028.
[28] Czuma N, Zarębska K, Motak M, Gálvez ME, Da Costa P. Ni/zeolite X derived from fly ash as catalysts for CO2 methanation. Fuel 2020;267:117139. https://doi.org/10.1016/j.fuel.2020.117139.
[29] Kiewidt L, Thöming J. Predicting optimal temperature profiles in single-stage fixed-bed reactors for CO2-methanation. Chem Eng Sci 2015;132:59–71. https://doi.org/10.1016/j.ces.2015.03.068.
[30] Falbo L, Martinelli M, Visconti CG, Lietti L, Bassano C, Deiana P. Kinetics of CO2methanation on a Ru-based catalyst at process conditions relevant for Power-to-Gas applications. Appl Catal B Environ 2018;225:354–63. https://doi.org/10.1016/j.apcatb.2017.11.066.
[31] Lunde PJ, Kester FL. Rates of methane formation from carbon dioxide and hydrogen over a ruthenium catalyst. J Catal 1973;30:423–9. https://doi.org/10.1016/0021-9517(73)90159-0.
[32] VDI-Verlag Gmbh. Heat exchanger design handbook. Hemisphere publishing corporation; 1983.
[33] Schlereth D. Kinetic and reactor modeling for the methanation of carbon dioxide. Technische Universität München; 2015.
[34] BOE-A-2013-185. Resolución de 21 de diciembre de 2012, de la Dirección General de Política Energética y Minas, por la que se modifica el protocolo de detalle PD-01. Energía y Turismo: Ministerio de Industria; 2013.